

NAR-*ICP: Neural Execution of Classical ICP-based Pointcloud Registration Algorithms

Efimia Panagiotaki^{1,2}, Daniele De Martini¹, Lars Kunze^{2,3}, Petar Veličković^{4,5}

Abstract

This study explores the intersection of neural networks and classical robotics algorithms through the Neural Algorithmic Reasoning (NAR) framework, allowing to train neural networks to effectively reason like classical robotics algorithms by learning to execute them. Algorithms are integral to robotics and safety-critical applications due to their predictable and consistent performance through logical and mathematical principles. In contrast, while neural networks are highly adaptable, handling complex, high-dimensional data and generalising across tasks, they often lack interpretability and transparency in their internal computations. We propose a Graph Neural Network (GNN)-based learning framework, NAR-*ICP, which learns the intermediate algorithmic steps of classical ICP-based pointcloud registration algorithms, and extend the CLRS Algorithmic Reasoning Benchmark with classical robotics perception algorithms. We evaluate our approach across diverse datasets, from real-world to synthetic, demonstrating its flexibility in handling complex and noisy inputs, along with its potential to be used as part of a larger learning system. Our results indicate that our method achieves superior performance across all benchmarks and datasets, consistently surpassing even the algorithms it has been trained on, further demonstrating its ability to generalise beyond the capabilities of traditional algorithms. We will make the code available for NAR-*ICP and the dataset generation on github.com/ori-mrg.

Keywords

Neural algorithmic reasoning, pointcloud registration, robotics perception, classical algorithms, iterative graph learning

1 Introduction

Algorithms serve as the foundation for tackling a wide range of robotics tasks, from path planning and optimisation to perception and control. Classical robotics algorithms are valued for their inherent modularity, ensuring reliable and consistent task execution. Their interpretable nature enables transparency and accountability in robotic operations, which are essential for understanding and validating the behaviour of robotic systems. However, traditional algorithms require strictly pre-defined data specifications, limiting their ability to process raw inputs and handle complex datasets.

Neural networks, in contrast, excel in efficiently handling raw sensor inputs and demonstrate robustness to noisy and complex data. By learning intricate patterns and dependencies within the input datasets, neural networks effectively generalise, performing reliably even in diverse and previously unseen scenarios. However, they lack interpretability, which poses challenges for transparent and accountable robotics operations.

Traditionally, neural networks have been trained using the ground truth directly as the supervisory signal, establishing direct mappings from raw inputs to the respective outputs without providing insights into their internal computational steps. This approach often leaves a gap in understanding the decision-making processes of these models. Aiming to combine the strengths of classical algorithms and neural networks, the Neural Algorithmic Reasoning (NAR) (Veličković and Blundell 2021; Veličković et al. 2020) framework integrates algorithmic computations within the latter. NAR achieves this by training a network to robustly approximate an algorithm by teaching it to mimic its reasoning through the intermediate algorithmic steps and outputs (Numeroso et al. 2023). This hybrid approach

offers flexible, scalable, and robust operation in complex and diverse inputs, robustness to noise and variability, and interpretable behaviour for prior black-box models. These features make this method well-suited for a wide range of tasks while bridging the gap between traditional algorithms and neural networks in robotics.

In this work, we focus on classical robotics perception algorithms, specifically addressing pointcloud registration as the primary task to be solved with NAR. We focus on Iterative Closest Point (ICP)-based algorithms as they are a fundamental methodology for rigid registration, widely accepted and used in robotics (Zhang et al. 2021). In addition, the compositional structure and iterative nature of ICP-based algorithms closely align with the characteristics of the algorithms in the CLRS Algorithmic Reasoning Benchmark (Veličković et al. 2022), making them a strong candidate for extending the latter in the robotics domain. Here, we train Graph Neural Networks (GNNs) to mimic these traditional pointcloud registration algorithms on various complex and real-world datasets, inheriting the interpretability of the algorithms within the networks and surpassing their performances.

¹Mobile Robotics Group (MRG), University of Oxford

²Cognitive Robotics Group (CRG), University of Oxford

³Bristol Robotics Laboratory (BRL), University of the West of England

⁴Google DeepMind

⁵University of Cambridge

Corresponding author:

Efimia Panagiotaki, Mobile Robotics Group and Cognitive Robotics Group, Oxford Robotics Institute (ORI), University of Oxford, Oxford, OX2 6NN, United Kingdom

Email: efimia@robots.ox.ac.uk

Our key contributions are as follows:

1. A novel NAR-based methodology for pointcloud registration, iteratively trained on intermediate algorithmic outputs, that effectively learns to reason like the algorithms by executing their intermediate steps while generalising and improving their performance.
2. An extension of the NAR framework and the CLRS Benchmark to robotics, introducing ground truth optimisation and learned termination, while validating its performance as part of a larger learning system.
3. A comprehensive evaluation and comparison of the neural execution of various fundamental ICP-based algorithms using complex and noisy data from synthetic and real-world datasets.

To the best of our knowledge, this is the first work applying NAR to a fundamental robotics perception task and the first to apply NAR to a task of this complexity.

The remainder of the paper is organised as follows: Section 2 frames this work in the literature, while Section 3 explains the background on NAR and the foundational techniques used. Section 4 details the methodology and key contributions. Section 5 describes the datasets, algorithms, and experimental setup, and Section 6 presents the experiments and results, showcasing the findings and discussing their significance. Section 7 proposes ablations to examine the contributions of different components to our model, and Section 8 discusses the integration of NAR-^{*}ICP into learning pipelines. Finally, Section 9 concludes the paper with a summary of our contributions, outlining potential directions for future research.

2 Related Work

This work intersects three key domains: robot learning, neural algorithmic reasoning, and pointcloud registration. In this section, we provide a brief overview of relevant works within each field, highlighting those that have particularly influenced our approach. We also discuss how our proposed method differs from and builds upon existing research.

Robot Learning. Learning methods in robotics have shown significant advancements, enabling robots to adapt to complex and dynamic environments. Imitation learning mimics expert demonstrations, reducing the need for extensive trial-and-error training (Billard and Grollman 2012; Celemin et al. 2022). On the other hand, reinforcement learning allows robots to learn optimal policies through trial-and-error (Kober et al. 2013; Singh et al. 2022). Transfer learning techniques enable robots to transfer knowledge acquired in one task to another, significantly improving learning efficiency and performance in new tasks (Zhuang et al. 2020). Meanwhile, in multi-task learning, robots learn multiple tasks simultaneously, sharing knowledge across to enhance overall learning efficiency (Zhang and Yang 2021). In recent years, foundation models have demonstrated impressive performance in multiple domains, leveraging extensive pre-training on large datasets to develop versatile representations which can be fine-tuned for specific applications (Firoozi et al. 2023). Alternatively, GNNs learn rich representations of spatial, temporal, and

relational data to address complex tasks (Pistilli and Averta 2023). Graph learning fundamentally interprets relationships between interconnected entities represented in graph form by iteratively aggregating information from related elements, effectively capturing complex relationships in datasets. In our proposed methodology, we leverage NAR and iterative deep graph learning (Chen et al. 2020b), integrating various pointcloud registration algorithms in the CLRS Benchmark (Veličković et al. 2022).

Neural Algorithmic Reasoning. Recent studies propose the concept of algorithmic alignment, suggesting that aligning the learning process with the steps of a target algorithm facilitates optimisation (Xu et al. 2020). NAR (Veličković and Blundell 2021) relies on the convergence of neural networks, and recently GNNs (Veličković et al. 2020), with classical algorithms, without relying on large datasets. A key distinction from traditional learning frameworks is that NAR models focus on learning and executing intermediate algorithmic steps rather than simply mapping inputs to outputs. NAR models leverage the flexibility of neural networks to learn intricate patterns and relationships within noisy and complex input data while training the networks to learn intermediate algorithmic computations. Studies demonstrate the effectiveness and usability of this framework in domains such as deep reinforcement learning (Deac et al. 2020), compositional dual reasoning (Numeroso et al. 2023), planning and decision-making (Deac et al. 2021; He et al. 2022), and explainability (Georgiev et al. 2022). Recent advancements combine language models with NAR by integrating the embeddings generated from both the transformers and NAR into a cross-attention layer (Bounsi et al. 2024). In this work, we extend the NAR framework and the CLRS Benchmark (Veličković et al. 2022), integrating complex multi-step pointcloud registration algorithms and optimising the output using ground truth supervisory signals and a termination network. We evaluate our approach on various challenging synthetic and real-world datasets, and test our method as part of a larger learning system.

Pointcloud Registration. The ICP algorithm (McKay N. 1992; Bai 2023) is considered one of the fundamental algorithms in the field of robotics and is widely used to solve rigid registration tasks (Rusinkiewicz and Levoy 2001; Pomerleau et al. 2013). ICP iteratively finds correspondences between two sets of points and estimates the relative transformation between them to eventually align them. Multiple methods have extended ICP to address different robotics challenges, such as handling noise and outliers in input data (Vizzo et al. 2023; Saleh and Momeni 2024; Segal et al. 2010), dealing with non-rigid deformations (Amberg et al. 2007; Li et al. 2008), faster registration (Zhang et al. 2021; Y. Chen and G. Medioni 1991), and integrating with other perception algorithms for autonomous navigation (Mendes et al. 2016). Deep learning has also been employed for learned pointcloud registration with methods such as GeoTransformer (Qin et al. 2022), TMP (Pramatarov et al. 2024), DCP (Wang and Solomon 2019), MDGAT (Shi et al. 2021), and DeepICP (Lu et al. 2019) that aim to find strong correspondences in feature space. Although these methods perform well, they are trained directly on ground truth data and lack transparency and interpretability. In this work, we use ICP as the supervisory signal for training GNNs to

learn the intermediate algorithmic steps, thus grounding the networks in the underlying algorithmic reasoning.

3 Preliminaries on NAR

This section summarises the variation of the NAR framework used, focusing on the components that are of most interest for the following discussion, and introduces the notation used throughout the paper. This section is by no means an exhaustive description of NAR, and we invite the reader to consult the original work (Veličković and Blundell 2021; Veličković et al. 2020; Ibarz et al. 2022) for a more in-depth discussion.

The NAR framework proposes to approximate a specific algorithm \mathcal{A} by mimicking not only its final output but also its intermediate state – or *steps* – by using its intermediate outputs as supervisory signals. In NAR, the steps of the algorithm can be represented as a graph, here denoted as a sequence $\mathbf{G} = \{G^{(0)} \dots G^{(T)}\}$, where $T \in \mathbb{N}$ is the final step of the algorithm, i.e. its *termination*. At each step $t \leq T$, the graph $G^{(t)}$ is described as $G^{(t)} = (V^{(t)}, E^{(t)}, x_i^{(t)}, e_{ij}^{(t)}, g_k^{(t)})$, where V and E are the nodes and edges, and x_i, e_{ij}, g_k are the node, edge, and graph features respectively. The initial graph $G^{(0)}$ at the first algorithmic step is the *input* to the network, and the last graph $G^{(T)}$ is the final *output* of \mathcal{A} .

At each step, t , the algorithm \mathcal{A} produces results $y^{(t)}$ that are used as target outputs for a GNN model to iteratively learn the sequential steps of the algorithm – i.e. its *trajectory* – by learning node, edge, and graph feature representations at each step to predict the next. The GNN follows the *encode-process-decode* paradigm introduced in (Hamrick et al. 2018) and implemented in (Veličković et al. 2020; Ibarz et al. 2022). Figure 1 depicts the relation between the algorithm and the learning iterations, while Figure 2 illustrates the *encoder-processor-decoder* and GNN message-passing methodology.

Encoders. To process the input features, we define linear *encoders* \mathbf{f}_v , \mathbf{f}_e , and \mathbf{f}_g for each x_i, e_{ij}, g_k to generate their corresponding embedded representations in node, edge, and graph level, respectively:

$$\begin{aligned} Z_V^{(t)} &= \{z_i^{(t)} = \mathbf{f}_v(x_i^{(t)}) \mid \forall x_i^{(t)} \in V^{(t)}\} \\ Z_E^{(t)} &= \{z_{ij}^{(t)} = \mathbf{f}_e(e_{ij}^{(t)}) \mid \forall e_{ij}^{(t)} \in E^{(t)}\} \\ Z_G^{(t)} &= \{z_k^{(t)} = \mathbf{f}_g(g_k^{(t)}) \mid \forall g_k^{(t)} \in G^{(t)}\} \end{aligned} \quad (1)$$

We call the collection of such embeddings $Z^{(t)}$.

Processor. The *processor* network is a GNN and is responsible for the major part of the learning process. It takes as input the embedding $Z^{(t)}$ from the current step, as well as the previous latent features $H^{(t-1)}$ to compute the latent features from the current step using MPNN (Gilmer et al. 2017; Veličković et al. 2022):

$$H^{(t)} = \mathbf{P}(Z^{(t)}, H^{(t-1)}) \quad (2)$$

Where for each node:

$$\begin{aligned} h_i^{(t)} &= \mathbf{f}_r(z_i^{(t)} \| h_i^{(t-1)}, m_i^{(t)}) \\ m_i^{(t)} &= \max_{1 \leq j \leq n} \mathbf{f}_m(z_i^{(t)} \| h_i^{(t-1)}, z_j^{(t)} \| h_j^{(t-1)}, z_{ij}^{(t)}, z_k^{(t)}) \end{aligned} \quad (3)$$

Here, \mathbf{f}_m is the message-passing function of the MPNN, \mathbf{f}_r is the readout function, and the embedding calculations start with $h_i, h_{ij} = \underline{0} \ \forall h_i, h_{ij} \in H^{(t-1)}$ in the input step $t = 0$ (Ibarz et al. 2022). As our task requires both edge and node-level reasoning, message-passing needs to also be performed in the edge embeddings (Dudzik and Veličković 2022), through *triplet reasoning* (Ibarz et al. 2022). Following the architecture of Triplet-MPNN, we compute representations over node-edge-node triplets, to obtain edge embeddings:

$$t_{ij} = \mathbf{t}_e(h_i, h_j, z_{ij}^{(t)}, z_g^{(t)}) \quad \text{and} \quad h_{ij} = \mathbf{t}_r(\max t_{ij}) \quad (4)$$

Where \mathbf{t}_e is a function that generates the triplet embeddings and \mathbf{t}_r is a readout function used to extract each respective edge embedding.

Decoders. The *decoders*, \mathbf{g}_v , \mathbf{g}_e , and \mathbf{g}_g , then decode the outputs for each step as:

$$\begin{aligned} \hat{x}_i^{(t+1)} &= \mathbf{g}_v(\hat{z}_i^{(t)}, h_i^{(t)}), \\ \hat{e}_{ij}^{(t+1)} &= \mathbf{g}_e(\hat{z}_{ij}^{(t)}, h_{ij}^{(t)}), \\ \hat{g}_k^{(t+1)} &= \mathbf{g}_g(\hat{z}_k^{(t)}) \end{aligned} \quad (5)$$

We call the collection of these outputs $\hat{y}^{(t)}$. Each decoded output effectively corresponds to the predicted input graph representation of the next step.

4 Methodology

In this section, we introduce NAR-*ICP¹ and detail the specific modifications and extensions made to the standard NAR framework to enable learning of complex robotics algorithms, such as ICP.

4.1 Pointcloud Registration

Pointcloud registration algorithms take as input two scans captured at different timesteps m and n , represented as $P_m = \{\mathbf{p}_i \mid \mathbf{p}_i \in \mathbb{R}^3\}$ and $P_n = \{\mathbf{p}_j \mid \mathbf{p}_j \in \mathbb{R}^3\}$ where each $\mathbf{p}_i, \mathbf{p}_j$ represents a point in three-dimensional space. We assume that P_n is transformed from P_m by a rigid transformation denoted by $[\mathbf{R}_{m,n} \mid \mathbf{t}_{m,n}]$, where $\mathbf{R}_{m,n} \in SO(3)$ is an orthogonal matrix representing the rotation of a point and $\mathbf{t}_{m,n} \in \mathbb{R}^3$ is a translation vector representing the displacement of the points in 3D space. ICP-based algorithms, here \mathcal{A} , aim to minimise the difference between P_n and the transformed P_m by iteratively minimising an error function $\mathbf{e}^{(t)}$, following a two-phase process. First, they find correspondences $C^{(t)} = \{(\mathbf{p}_i, \mathbf{p}_j) \mid \mathbf{p}_i \in P_m, \mathbf{p}_j \in P_n\}$ by matching each point in P_n to a point in P_m . Then, they leverage these correspondences to estimate the relative transformation that aligns the pointclouds. This iterative process continues until the error criterion \mathbf{e} is minimised or until the algorithm reaches a predefined maximum number of iterations. The general structure of ICP-based algorithms is detailed in the pseudocode in Algorithm 1.

¹The asterisk (*) in NAR-*ICP refers to the different ICP-based algorithms that are approximated using NAR in this paper.

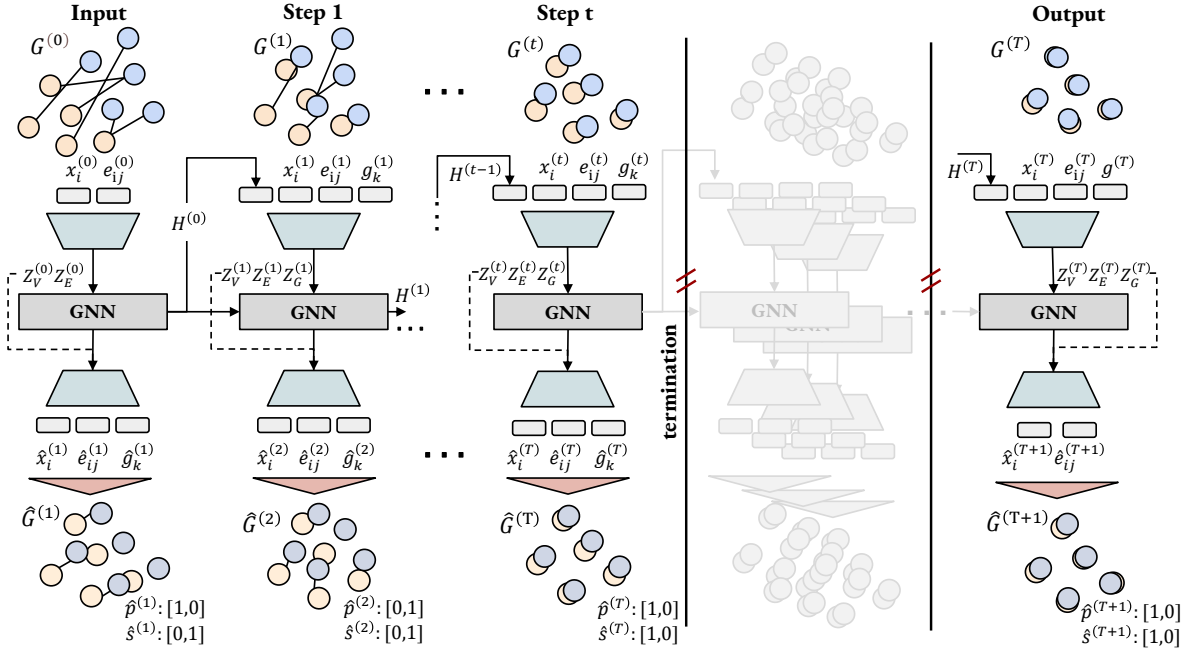


Figure 1. Learning process: Each output of the algorithm is converted into a graph representation, $G^{(t)} = (V^{(t)}, E^{(t)}, x_i^{(t)}, e_{ij}^{(t)}, g_k^{(t)})$, before being passed to an *encoder-processor-decoder* model. The encoder generates embedding representations from the input features, $Z^{(t)}$, which are then used in a Triplet Message-Passing Neural Network (MPNN) to generate latent features $H^{(t)}$. These features are passed to a decoder that predicts the features, $\hat{y}^{(t)}$, that effectively correspond to the output of the algorithm at step t . The process is repeated for all intermediate steps of the algorithm. The model additionally learns a phase, $\hat{p}^{(t)}$, and a termination, $\hat{s}^{(t)}$, flag, as independent binary classes, predicting the different phases of the algorithm – finding correspondences and estimating relative transformation and error – and its final step. During inference, when the termination flag is triggered, the algorithmic execution terminates at $\hat{y}^{(T)}$. Additionally, we leverage the ground truth from each input dataset as a final training signal to optimise the model’s output $\hat{y}^{(T+1)}$, on the right.

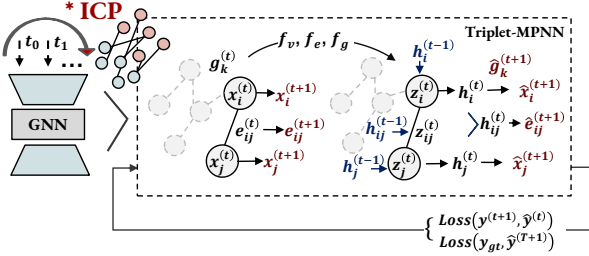


Figure 2. At each algorithmic step, we encode the input features, $x_i^{(t)}, x_j^{(t)}, e_{ij}^{(t)}$, and $g_k^{(t)}$, and use the latent features from the previous step of the processor to generate the current step’s latent representations. In this context, $h_i^{(t)}$ and $h_j^{(t)}$ correspond to the node features, while $h_{ij}^{(t)}$ denotes the edge features, which result from the aggregation of node and graph encodings. The loss is calculated between the decoder’s output $\hat{y}^{(t)}$ and the output of the algorithm $y^{(t)}$ at each iteration. Our method uses the ground truth from the input dataset y_{gt} as an additional optimisation step $t = T + 1$.

4.2 Neural Execution of Pointcloud Registration

To learn to execute the intermediate algorithmic steps and reason like pointcloud registration algorithms, we represent the input, output, and transformed pointclouds as graphs with the same structure but different features corresponding to the execution steps of the algorithm. The input, output, and intermediate steps of the algorithm are passed to the model as *probes* – i.e. the learning signals – with the intermediate steps specifically referred to as *hints* (Veličković et al. 2022).

Algorithm 1 ICP-based Algorithms

— Phase 1 — Phase 2

Inputs: Pointclouds src, tgt

Outputs: Transformation between pointclouds T

```

1: iter = 0, error = ∞
2: while error > tolerance and iter < max_iter do
3:   adj = GetCorrespondences(src, tgt)
4:   T = GetTransform(src, tgt, adj)
5:   error = GetError(T(src), tgt)
6:   if error > tolerance then
7:     iter = iter + 1
8:     src = T(src)
9:   end if
10: end while
11: return T

```

Graph Representations and Probes. In our model, the points in the two pointclouds, P_m and P_n , compose the nodes $V^{(t)}$ and the correspondences between them are the edges $E^{(t)}$ for each graph $G^{(t)}$. Each element in $G^{(t)}$ corresponds to a probe in NAR-*ICP, as seen in Table 1.

At the first step, $t = 0$, we represent the initial pointclouds, P_m and P_n , as nodes $V^{(0)}$ consisting of node features, $x_i^{(0)}$ and $x_j^{(0)}$, and pass them as input probes to the model. Then, at each consecutive step t , we convert the output of the algorithm to a graph and pass the nodes $V^{(t)}$ and edges $E^{(t)}$, along with the graph $g_k^{(t)}$, node $x_i^{(t)}$ and $x_j^{(t)}$, and edge $e_{ij}^{(t)}$ features, as a sequence of *hints*. Edge features, $e_{ij}^{(t)}$, are set to the distance in Euclidean space of the nodes $x_i^{(t)}$ and

Table 1. Input, hints, and output probes, probe types, and associated graph features in NAR-*ICP.

	Probe	Feature	Type
Input	Pointclouds	x_i^0, x_j^0	scalar
	Node positions	V^0	scalar
Hints	Transformed Pointclouds	$x_i^{(t)}, x_j^{(t)}$	scalar
	Correspondences	$E^{(t)}$	mask
	Distances	$e_{ij}^{(t)}$	scalar
	Error	$g_k^{(t)}$	scalar
	Iterations	$g_k^{(t)}$	scalar
	Phase	$g_k^{(t)}$	categorical
	Stop	$g_k^{(t)}$	categorical
Output	Final Pointclouds	$x_i^{(T)}, x_j^{(T)}$	scalar
	Final Correspondences	E^T	mask

$x_j^{(t)}$. To showcase the flexibility of our method, we design different feature representations for $x_i^{(t)}$ and $x_j^{(t)}$ – namely three dimensional spatial data, spatial data augmented with high-level semantics, and contrastively learned features.

Finally, we define graph features, $g_k^{(t)}$, containing the iterations termination criteria of the algorithm: error $e^{(t)}$ and iterations counter. The error corresponds to the convergence criterion of the algorithm based on a pre-defined tolerance threshold. The iterations counter contains the number of repetitive steps performed by the algorithm to refine the alignment between the two pointclouds.

Separate from the algorithmic calculations, we introduce two additional hint probes, phase and stop, and represent them as graph features $g_k^{(t)}$. As ICP-based algorithms are modular, the phase hint identifies the two main phases: finding correspondences and estimating the relative transformation and error between them. The stop hint guides the termination network and indicates the iteration at which the algorithm terminates.

Probe Types. Depending on the type of features they hold, probes are further split into *node*, *edge*, and *graph* probes to ensure data are being distributed and handled appropriately in the GNN. Probes are categorised into *scalar*, *mask*, and *categorical*, following the CLRS Benchmark (Veličković et al. 2022). Specifically, in NAR-*ICP, probes are categorised as follows:

- *Scalar* probes refer to regressed floating point variables, either in scalar or vectorial form. Here, these correspond to the pointclouds, the node positions², the relative distances between correspondences, the error, and iterations.
- *Mask* probes correspond to binary categorical features. In our method, these are the correspondences implemented as adjacency matrices.
- *Categorical* probes are k-class categorical features. In our case, they are used for the phase and stop signals; thus $k = 2$.

Here, we extend the CLRS benchmark to include scalar probes in the output of the NAR processes.

We normalise all input scalar probes, apart from error, using min-max scaling to ensure each feature contributes

Algorithm 2 Probes and hint updates* for generating the supervisory signals for NAR-*ICP.

— Phase 1 — Phase 2 *denoted by \leftarrow assignment

Input: Pointclouds src, tgt . Node positions pos .
Hints: Pointclouds $\text{src}_h, \text{tgt}_h$. Correspondences adj_h . Distances dist . Iterator iter . Error error . Phase phase . Termination stop .
Output: Final pointclouds $\text{src}_{\text{final}}, \text{tgt}_{\text{final}}$. Final correspondences $\text{adj}_{\text{final}}$

```

1:  $\text{stop} \leftarrow \text{False}, \text{error} \leftarrow \infty, \text{iter} \leftarrow 0$ 
2: while  $\text{error} > \text{tolerance}$  and  $\text{iter} < T_{\text{max}}$  do
3:    $\text{phase} \leftarrow 0$ 
4:    $\text{adj}_h \leftarrow \text{GetCorrespondences}(\text{src}_h, \text{tgt}_h)$ 
5:    $\text{dist} \leftarrow \|(\text{src}_h - \text{tgt}_h)\|_{\text{adj}_h}$ 
6:    $\text{phase} \leftarrow 1$ 
7:    $\text{T} \leftarrow \text{GetTransform}(\text{src}_h, \text{tgt}_h)_{\text{adj}_h}$ 
8:    $\text{error} \leftarrow \text{GetError}(\text{T}(\text{src}_h), \text{tgt}_h)$ 
9:   if  $\text{error} > \text{tolerance}$  then
10:     $\text{dist} \leftarrow \|(\text{T}(\text{src}_h) - \text{tgt}_h)\|_{\text{adj}_h}$ 
11:     $\text{src}_h \leftarrow \text{T}(\text{src}_h)$ 
12:     $\text{iter} \leftarrow \text{iter} + 1$ 
13:   else
14:     $\text{stop} \leftarrow \text{True}$ 
15:     $\text{T}_{\text{final}}, \text{adj}_{\text{final}} = \text{T}, \text{adj}_h$ 
16:     $\text{src}_{\text{final}} = \text{T}_{\text{final}}(\text{src}_h)$ 
17:   end if
18: end while
19: if  $\text{gt\_optimisation}$  then
20:    $\text{T}_{\text{final}}, \text{adj}_{\text{final}} = \text{GetGT}(\text{src}, \text{tgt})$ 
21:    $\text{src}_{\text{final}} = \text{T}_{\text{final}}(\text{src})$ 
22:    $\text{tgt}_{\text{final}} = \text{tgt}$ 
23: end if
24: return  $\text{src}_{\text{final}}, \text{tgt}_{\text{final}}, \text{adj}_{\text{final}}$ 

```

equally to the learning process and to improve the convergence speed and stability of the training. To ensure the error probe falls within the normalisation boundaries for a maximum tolerance of 10^{-10} , we adjust its value as follows:

$$f_e(e) = \frac{1}{1 + e^{-\log(e)+c}} \quad (6)$$

Here, $c = 5$ is responsible for adjusting the input range for the sigmoid function and controlling the sensitivity of the changes of e . This sigmoid transformation effectively maps the tolerance into a range of (0,1) with the behaviour controlled by the magnitude of e .

Hint Updates. All key algorithmic computations are encapsulated in the hint probes, used as training signals for NAR-*ICP. Hints capture the trajectory of the algorithms and thus reflect the different aspects of their internal computations. While ICP-based algorithms are structurally similar, as seen in Algorithm 1, the specific intermediate outputs and calculations –such as error and relative transformation computations– generate distinct hint trajectories for each variant. To effectively train NAR-*ICP to mimic the behaviour of the algorithms, we aim to capture as many algorithmic details as possible in the hint update configuration. We provide a pseudocode, in Algorithm 2, illustrating the modifications made to Algorithm 1 in order to perform the appropriate hint updates for NAR-*ICP. In

²Node positions, guided by the node indices, are used in CLRS to generate positional encodings for each input node.

Algorithm 2, node hints are highlighted in **blue**, edge hints in **red**, and graph hints in **green**.

In particular, to capture the behaviour and intermediate computations of the two-phase ICP-based algorithms in this study, we update the hints after each phase. Here, *Phase 1* denotes the correspondence-finding phase, in **GetCorrespondences**, and *Phase 2* the relative transformation and error estimation phase, in **GetTransform** and **GetError**. The second phase is different for each algorithm. During inference, the **phase** hint predictions allow us to identify the intermediate components of the algorithmic execution, while the **stop** hint predictions determine the termination of the processor’s iterations.

In ICP-based algorithms, there are multiple control flow statements that generate different algorithmic trajectories. As GNNs operate on parallelised architectures, we “compressed” the hints to align with the network’s training behaviour while still capturing succinct yet descriptive algorithmic trajectories. For instance, in the correspondence-finding phase, each point in **tgt_h** is iteratively compared to the points in **src_h** to find its nearest neighbour. Following the parallelised nature of the underlying network, we optimise this process by passing only the resulting correspondences as an adjacency matrix, **adj_h**, and the distance matrix of the correspondences, **dist**, within the hints trajectory. Similarly, after estimating the relative transformation between the two pointclouds, we transform **src_h** and update the hint.

The intermediate algorithmic steps, denoted as t , that guide the iterative training process of the network, effectively capture the evolving trajectory of the algorithm as it progresses through each phase on every iteration. This process continues until the algorithmic termination criteria are met. In particular, the algorithm terminates if the **error** drops below the **tolerance** threshold or if **iter** reaches the maximum number of iterations in **T_{max}**.

In NAR-*ICP, we introduce an additional optimisation step using the ground truth obtained from the input datasets. In the **GetGT** function, we use the ground truth relative transformation to find the ground truth correspondences. To do so, we transform the initial **src** pointcloud using the ground truth relative transformation to align the two pointclouds. Then, for each point in the transformed **src**, we find its closest points in **tgt** and extract the ground truth correspondences. If the **gt_optimisation** flag is triggered, we pass the transformed **src**, the **tgt**, and the ground truth correspondences as output probes **src_{final}**, **tgt_{final}**, and **adj_{final}**, respectively. If the flag is not triggered, we pass the output of the algorithm as the output probes.

Termination. In CLRS (Veličković et al. 2022), the number of processor steps during testing and evaluation is determined by the number of hints. In NAR-*ICP, we introduce a separate termination criterion that effectively predicts a binary flag that indicates the last step of the algorithm. This network is trained in the processor using a separate mask probe through the **stop** hint and gets encoded as a graph probe alongside other termination criteria, i.e. **error**, **iter**, and **phase**. We train the termination network using binary classification. Using the network’s predictions, the processor dynamically adjusts the number of iterations required during inference, thus avoiding unnecessary computations and improving the

overall efficiency and convergence of the iterative process. In particular, the termination network predicts the probability of each iteration being the final step of the algorithm and, consequently, the termination step of the processor, effectively halting further iterations.

Training. Each type of probe is handled differently during training, both in the *encoder-processor-decoder*, and the loss calculations, depending on whether it belongs to the node, edge, or graph probes, and its specific data type, i.e. scalar, mask, or categorical.

In the *encoder-processor-decoder*, node features are initially encoded individually, updated through message-passing between node, edge, and graph features, and then decoded into node-specific outputs. Edge features are encoded, capturing relationships between node pairs, and then get iteratively updated, forming triplets of node-edge-node pairs before being decoded. Graph features are encoded and updated globally, aggregating information from across the graph, and finally, get decoded into global outputs that represent overall graph properties. This process is further described in Section 3.

In the loss calculation, the scalar, mask, and categorical features define the type of loss to be applied to each type of probe. In particular, for each hint and output probe, we compare the values extracted from the decoders’ predictions $\hat{y}^{(t)}$ with the ground truth hints $y^{(t)}$ at each processor step t and calculate the appropriate loss depending on its type. The losses used in NAR-*ICP are as follows:

- For the *scalar* probes, we apply a Mean Squared Error (MSE) loss with a scaling factor α to balance the loss terms and stabilise the training:

$$\mathcal{L}_{\text{scalar}}^{(t)} = \alpha \frac{1}{|Y_s|} \sum_{y_i \in Y_s} \|y_i^{(t)} - \hat{y}_i^{(t)}\|_2 \quad (7)$$

where Y_s is the set of scalar variables in y .

- For the *mask* probes, we introduce the set of mask variables Y_m , in y and apply a weighted Binary Cross Entropy (BCE) loss:

$$w_{\text{pos}}^{(t)} = \frac{\sum_{y_i \in Y_m} \mathbb{I}(y_i^{(t)} = 0)}{\sum_{y_i \in Y_m} \mathbb{I}(y_i^{(t)} = 1) + \epsilon} \quad (8)$$

$$\begin{aligned} \mathcal{L}_{\text{mask}}^{(t)} = -\frac{1}{|Y_m|} \sum_{y_i \in Y_m} & \left(w_{\text{pos}} y_i^{(t)} \log(\hat{y}_i^{(t)}) \right. \\ & \left. + (1 - y_i^{(t)}) \log(1 - \hat{y}_i^{(t)}) \right) \end{aligned} \quad (9)$$

Here \mathbb{I} corresponds to the indicator function.

- For the *categorical* probes, we apply a Categorical Cross Entropy (CCE) loss with Y_c the set of scalar variables in y :

$$\mathcal{L}_{\text{categ}}^{(t)} = - \sum_{y_i \in Y_c} \sum_{c \in k} y_{i,c}^{(t)} \log(\hat{y}_{i,c}^{(t)}) \quad (10)$$

We also introduce an optimisation step to our training process, as described previously. This includes passing the ground truth transformed pointclouds and correspondences as additional training signals in the final step of the model

and computing an additional loss term, as shown in the last lines of Algorithm 2. We retrieve the ground truth information from the input datasets. The last step of our model is then trained conditionally:

$$\mathcal{L}_{final} = \begin{cases} \mathcal{L}(\hat{y}^{(t)}, y_{gt}), & t = T + 1 \\ \mathcal{L}(\hat{y}^{(t)}, y^{(t)}), & t = T \end{cases} \quad (11)$$

Here, \mathcal{L} corresponds to the \mathcal{L}_{scalar} loss for the pointclouds and the \mathcal{L}_{mask} loss for the correspondences. We retrieve the ground truth transformed source pointclouds as $P_{gt} = R_{gt}P_m + t_{gt}$, and then find the closest points between P_n and P_{gt} to extract the ground truth adjacency matrix, adj_{gt} .

To ensure input hints are being encoded in each step of the processor, we use *teacher-forcing* (Godwin et al. 2022) where we feed back the ground truth hints in the input during training to stabilise the trajectory of the hints. Naturally, this is done only during training as, during inference, the encoded hints are equal to the decoded hints of the previous step.

Due to the recursive nature of NAR, the issues of exploding and vanishing gradients are prominent during training. To tackle these, we apply Xavier initialisation (Glorot and Bengio 2010) on the scalar hints and gradient clipping (Pascanu et al. 2013). Xavier (or Glorot) initialisation sets the initial weights of the network to preserve the variance of activations across layers. Gradient clipping caps the gradients during backpropagation to prevent exploding gradients, which occurred due to the large number of iterations when training NAR- \ast ICP. We also apply layer normalisation in the iterative model to stabilise the learning process further and enhance generalisation.

5 Experimental Setup

In this section, we discuss our experimental setup, detailing the specific algorithms, datasets, tools, and configurations used to evaluate our approach.

5.1 Algorithms

As our approach is generic for pointcloud registration, we evaluated it in approximating several algorithms of the ICP family: point-to-point ICP (P2P-ICP) McKay N. (1992), point-to-plane ICP (P2L-ICP) Y. Chen and G. Medioni (1991), and Generalised-ICP (G-ICP) Segal et al. (2010). These algorithms will also constitute the baselines against which we evaluate our method. While all calculate correspondences $C^{(t)}$ at each iteration as the closest points in the transformed P_m for each point in P_n in Euclidean space, they differ in the calculation of the relative transformation $[R_{m,n}^{(t)} | t_{m,n}^{(t)}]$ and the error $e^{(t)}$. The iterative process repeats until convergence, i.e. the transformation estimations stabilise and the error is minimised. Please refer to Algorithm 1 for an overview of the generic ICP operations.

Point-to-point ICP. After finding correspondences $C^{(t)}$, P2P-ICP estimates the relative transformation between them, $[R_{m,n}^{(t)} | t_{m,n}^{(t)}]$, through Singular Value Decomposition (SVD). The transformation is then used to transform P_m , and the process repeats until it minimises the sum of square distances between corresponding points, denoted as the error:

$$e^{(t)} = \sum_{(\mathbf{p}_i, \mathbf{p}_j) \in C^{(t)}} \|\Delta_{ij}^{(t)}\|_2 \quad (12)$$

We define $\Delta_{ij}^{(t)}$ as the vectorial distance between each set of points $(\mathbf{p}_i, \mathbf{p}_j) \in C^{(t)}$, as:

$$\Delta_{ij}^{(t)} = \mathbf{R}_{m,n}^{(t)} \mathbf{p}_i + \mathbf{t}_{m,n}^{(t)} - \mathbf{p}_j \quad (13)$$

Point-to-plane ICP. At each iteration, P2L-ICP minimises the distance between each point in P_n to the tangent plane of the corresponding transformed point in P_m , represented by its normal vector \mathbf{n}_j . The error $e^{(t)}$ is then computed as follows:

$$\mathbf{e}^{(t)} = \sum_{(\mathbf{p}_i, \mathbf{p}_j) \in C^{(t)}} \mathbf{n}_j \cdot \Delta_{ij}^{(t)} \quad (14)$$

where \cdot denotes the dot product. The algorithm minimises the point-to-plane error, $e^{(t)}$, by iteratively calculating the relative transformation and solving a linear system derived by the Jacobian J of the error $e^{(t)}$ until convergence.

Generalised-ICP. Relying on the covariance matrices of the correspondences, G-ICP minimises the Mahalanobis distance between corresponding points. The algorithm combines P2P-ICP and P2L-ICP into a single optimisation framework. We denote with $\mathbf{M}_{ij}^{(t)}$ the inverse covariance matrix between $(\mathbf{p}_i, \mathbf{p}_j) \in C^{(t)}$:

$$\mathbf{M}_{ij}^{(t)} = (\Sigma_{p_i}^{(t)} + \mathbf{R}_{m,n}^{(t)} \Sigma_{p_j}^{(t)} \mathbf{R}_{m,n}^{(t)T})^{-1} \quad (15)$$

where $\Sigma_{p_i}^{(t)}$ and $\Sigma_{p_j}^{(t)}$ are the covariance matrices of points in P_m and P_n , respectively. The error function $e^{(t)}$ is then defined as:

$$\mathbf{e}^{(t)} = \sum_{(\mathbf{p}_i, \mathbf{p}_j) \in C^{(t)}} \Delta_{ij}^{(t)T} \mathbf{M}_{ij}^{(t)} \Delta_{ij}^{(t)} \quad (16)$$

The gradient of $e^{(t)}$ is followed until convergence.

5.2 Datasets

To thoroughly test our system’s capabilities, we consider two distinct datasets: one synthetic and one real-world, each possessing very different characteristics.

Synthetic. We extend the CLRS Benchmark (Veličković et al. 2022) with a complex synthetic dataset consisting of random pointclouds with (x, y, z) coordinates uniformly distributed within the range $[-40, 40]$. Each pointcloud is part of a set where the second pointcloud is generated by applying a random relative transformation to the first. The synthetic dataset is particularly interesting as, due to the large relative transformation between the pointclouds, ICP-based algorithms are expected to underperform or even fail to reach convergence.

Real-World. Our real-world dataset consists of centroids of objects and associated semantic labels extracted from SemanticKITTI (Behley et al. 2019). Here, we define as *object* a local region in the scan with the same semantic class. To extract them, we cluster points within each semantic class based on spatial proximity, with constraints on minimum cluster size and maximum clustering tolerance as in (Kong et al. 2020; Panagiotaki et al. 2023). The centroids are then computed as the mean of the coordinates of all points belonging to an object. To assess the performance of our method, we evaluate our approach on scan pairs recorded at

various distances from each other. In particular, we measured registration performance on scans recorded 1.6 m, 11.3 m, and 24 m apart on average. In registration tasks, scans recorded further apart from each other are more challenging than scans recorded closer together due to the larger number of outliers and the mismatch between estimated and actual correspondences.

This dataset highlights the robustness of NAR-*ICP on complex and noisy data with outliers in the input. Moreover, we demonstrate the flexibility of our method in handling various types of inputs as we can solve the registration either using 3D coordinates alone for each centroid or by additionally including the associated semantic class. For the real-world datasets, we solve the algorithms using the pointclouds while additionally training the model using the semantics. Semantic data are passed as node probes and get encoded at each processing step along with the pointclouds.

5.3 Metrics

We employ several quantitative metrics to evaluate the performance and effectiveness of our proposed approach in comparison to the baselines. These metrics are applied to different combinations of outputs and target signals, as outlined below:

1. \star^T : The final step of the algorithmic execution, $\hat{y}^{(T)}$, as predicted from the termination, compared to the final step of the algorithm, $y^{(T)}$.
2. \star^t : Each step of the algorithmic execution, $\hat{y}^{(t)}$, compared to each step of the algorithm, $y^{(t)}$.
3. \star^{GT} : The final step of the algorithm, $y^{(T)}$, and the final step of the algorithmic execution – either before, as predicted from the termination, $\hat{y}^{(T)}$, or after training with ground truth optimisation, $\hat{y}^{(T+1)}$ – compared to the ground truth from the input dataset, y_{gt} .

We utilise the definition above and apply it to our metrics, each denoted with the corresponding superscript, e.g. $[\text{metric}]^T$.

Registration Accuracy. First, we assess the performance of our method as a pose regressor, which is the primary goal of pointcloud registration algorithms. We use the Relative Translation Error (RTE)(\downarrow) and Relative Rotation Error (RRE)(\downarrow) from the KITTI metrics (Geiger et al. 2013), where:

$$RTE(t) = \|t - \hat{t}\|, \quad RRE(R) = \arccos \frac{\text{Tr}(\hat{R}^\top R) - 1}{2} \quad (17)$$

Here, \hat{t} and \hat{R} are the estimated translation and rotation from the model, R , t are the ground truth values, and $\text{Tr}(\cdot)$ represents the trace of a matrix. Lower values in RTE and RRE metrics (Geiger et al. 2013) indicate better performance. We compare our approach against the original algorithm used for its training, in RTE^T and RRE^T , and the ground truth, in RTE^{GT} and RRE^{GT} . As NAR-*ICP outputs correspondences and transformed pointclouds, we need to extract the estimated relative transformation from the predictions. To retrieve the estimated translation and rotation, we apply SVD on the nodes corresponding to the predicted target P_n and transformed source \hat{P}_m pointclouds. These

metrics allow us to measure our method’s raw potential as a pose regressor by providing insights into how well the model can align two sets of 3D pointclouds.

Intermediate Hints. To evaluate the accuracy of the intermediate hints predictions, we extract the MSE^t error distributions of the predicted transformed pointclouds against those of the algorithm at each step of the algorithmic execution. We then compare the median and interquartile range (IQR) for the error distributions, as well as the number of outliers for each benchmark and dataset. Lower medians and smaller IQRs indicate lower overall error, suggesting better prediction accuracy. A smaller number of outliers reflects greater consistency and overall reliability in the model’s performance. This is critical for both pointcloud registration and for approximating the trajectory of an algorithm. In pointcloud registration, consistency and reliability directly impact the accuracy and usability of the models. For trajectory approximation, they signify how successfully the NAR-based models have learned to mimic the intermediate algorithmic steps. Thus, achieving both low error rates and minimal outliers is essential for optimal performance in these tasks.

Prediction Accuracy. We compare the predicted transformed pointclouds from NAR-*ICP and the output of the algorithms against the ground truth, by calculating the $\text{MSE}(\downarrow)$ scores. To retrieve the transformed pointclouds from the algorithm and the ground truth, we transform the source pointcloud P_m using the transformation matrices estimated by each. To then evaluate our models’ performance in identifying correct registration correspondences, we employ several key classification metrics(\uparrow): F1 score (F1), Precision (P), Recall (R), and Balanced Accuracy (A), similar to (Shi et al. 2021). These metrics, applied to imbalanced binary classification, provide a comprehensive assessment of the models’ predictive performance.

5.4 Training Details

To finalise the training configuration, we compared various network architectures, *teacher-forcing* probabilities, and hint configurations, as outlined in Section 7. During training, *teacher-forcing* was applied with a probability of $P_T = 0.1$ to stabilise the trajectories by feeding the ground truth hints back to the network at each step. We then used softmax for the categorical hints and sigmoids for the mask hints. For the synthetic dataset, 1000, 64, and 64 random samples were generated for training, evaluation, and testing, respectively. The real-world dataset was split using a 60/20/20 % split across graphs extracted from sequences 00, 02, 04, and 06 of SemanticKITTI. These sequences were selected due to the varying complexity of the routes and the diversity of the environment in each. Models were trained for 10 000 steps with a batch size of 8, calculating the loss for each intermediate hint and output. The hidden size for model features was set to 256, and the Adam optimiser was used with a learning rate of 1×10^{-3} . Finally, as the network requires fixed-length inputs, we adjust the number of the input nodes to ensure compatibility with the encoders’ architecture. To maintain consistency in the representations, especially when working with real-world datasets, we either pad the input nodes by randomly repeating them or randomly mask them, depending on the number of nodes in the input.

Table 2. Registration performance comparison, in $\text{RTE}^{\text{GT}}(\downarrow)$ and $\text{RRE}^{\text{GT}}(\downarrow)$, of the final step of the algorithm used as training signal and the final step of the algorithmic execution against the ground truth from the dataset. Across almost all datasets and benchmarks, our NAR-based models outperform the algorithms they were trained on, demonstrating our method’s strong generalisation capabilities.

Method	Synthetic		KITTI @ 1.6 m		KITTI @ 11.3 m		KITTI @ 24 m	
	RTE	RRE	RTE	RRE	RTE	RRE	RTE	RRE
P2P-ICP	0.859	1.654	0.402	0.800	1.003	2.007	0.934	1.912
NAR-P2Pv1	0.904	1.585	0.432	0.843	0.828	1.746	0.888	1.769
NAR-P2Pv2	0.822	1.798	0.651	1.127	0.769	1.643	0.894	1.769
P2L-ICP	0.986	2.092	0.446	0.993	1.147	2.043	1.032	2.050
NAR-P2L	0.346	0.626	0.177	0.345	0.496	0.785	0.391	0.796
G-ICP	0.901	2.063	0.518	1.232	1.022	2.168	0.944	1.981
NAR-GICP	1.037	2.022	0.550	1.131	0.857	1.789	0.616	1.628

Table 3. Registration performance comparison, in $\text{RTE}^{\text{GT}}(\downarrow)$ and $\text{RRE}^{\text{GT}}(\downarrow)$, of the final step of the algorithm and the final step of the algorithmic execution after ground truth optimisation against the ground truth from the dataset. Our optimisation step significantly improves the registration performance of the underlying algorithm.

Method	Synthetic		KITTI @ 1.6 m		KITTI @ 11.3 m		KITTI @ 24 m	
	RTE	RRE	RTE	RRE	RTE	RRE	RTE	RRE
P2P-ICP	0.859	1.654	0.402	0.800	1.003	2.007	0.934	1.912
NAR-P2Pv1 ⁺	0.246	0.496	0.138	0.245	0.287	0.574	0.261	0.496
NAR-P2Pv2 ⁺	0.267	0.531	0.156	0.302	0.204	0.386	0.241	0.480
P2L-ICP	0.986	2.092	0.446	0.993	1.147	2.043	1.032	2.050
NAR-P2L ⁺	0.274	0.533	0.127	0.221	0.279	0.542	0.274	0.493
G-ICP	0.901	2.063	0.518	1.232	1.022	2.168	0.944	1.981
NAR-GICP ⁺	0.292	0.579	0.175	0.328	0.276	0.556	0.222	0.458

Table 4. Registration performance comparison, in $\text{RTE}^{\text{T}}(\downarrow)$ and $\text{RRE}^{\text{T}}(\downarrow)$, of our methods when learning to approximate the final step of the algorithm. The simpler trajectory approximation method, NAR-P2Pv1, outperforms the more complex baselines.

Method	Synthetic		KITTI @ 1.6 m		KITTI @ 11.3 m		KITTI @ 24 m	
	RTE	RRE	RTE	RRE	RTE	RRE	RTE	RRE
NAR-P2Pv1	0.607	1.142	0.393	0.588	0.660	1.135	0.545	1.107
NAR-P2Pv2	0.637	1.268	0.514	0.781	0.823	1.447	0.713	1.383
NAR-P2L	0.952	2.066	0.464	1.029	1.254	2.057	1.114	2.102
NAR-GICP	0.890	1.641	0.485	0.876	0.947	1.681	0.875	1.578

6 Results

We compare the performance of our model against all baseline algorithms and their NAR approximation on our datasets. From P2P-ICP we learn two policies, NAR-P2Pv1 and NAR-P2Pv2, from P2L-ICP we learn NAR-P2L, and from G-ICP, NAR-GICP. These correspond to the neural execution of each algorithm, respectively. When the method is superscript with a +, such as NAR-GICP⁺, the model was trained with the additional ground truth optimisation step. For the neural execution of P2P-ICP, NAR-P2Pv1 and NAR-P2Pv2 differ in training strategy: NAR-P2Pv2 is trained to separately approximate the two phases of the algorithm, while NAR-P2Pv1 uses a single-phase approach containing only the output from the transformation and error estimation corresponding to the second phase of the algorithm. The other methods, NAR-P2L and NAR-GICP, follow the two-phase approach, similar to NAR-P2Pv2, ensuring a more comprehensive representation of the algorithm’s trajectory.

In the following, we compare the approaches both quantitatively and qualitatively against each other and the baseline algorithms. We evaluate our method in solving the registration task and in its effectiveness at approximating the underlying algorithms.

6.1 Registration Performance

Quantitative Results: Registration Accuracy. To evaluate the performance of our pointcloud registration method, we assess the RTE and RRE of different combinations of outputs and target signals, as defined in Section 5.3.

In Table 2, we compare the algorithmic performance and the algorithmic execution against the ground truth, in RTE^{GT} and RRE^{GT} . The results indicate that our NAR-based algorithmic execution, in most cases, outperforms the algorithm it was trained to approximate when comparing both with the ground truth. This behaviour is especially evident in more challenging datasets – such as synthetic and KITTI > 11.3 m – where the displacement between scans

Table 5. $MSE^T (\times 10^2) (\downarrow)$ of the predicted final transformed pointclouds. NAR-P2Pv1, NAR-P2Pv2, and NAR-P2L achieve comparable predictive performance across the datasets.

Method	Synthetic			KITTI @ 1.6 m			KITTI @ 11.3 m			KITTI @ 24 m		
	MSE_x	MSE_y	MSE_z	MSE_x	MSE_y	MSE_z	MSE_x	MSE_y	MSE_z	MSE_x	MSE_y	MSE_z
NAR-P2Pv1	1.792	2.386	2.267	1.114	0.744	0.619	1.970	1.824	1.718	2.986	2.138	1.682
NAR-P2Pv2	5.026	4.820	4.326	0.562	0.370	1.131	1.777	1.604	2.334	4.828	1.508	1.935
NAR-P2L	1.903	1.968	1.706	1.055	0.975	0.799	3.052	2.367	2.727	2.132	2.970	1.999
NAR-GICP	4.924	5.088	5.111	3.139	2.546	2.830	5.346	4.547	5.489	4.083	5.202	4.821

Table 6. Classification scores (\uparrow), $F1^T$, P^T , R^T , and A^T , of the predicted final correspondences. NAR-P2Pv1 demonstrates superior performance on the synthetic dataset, while NAR-P2Pv2 consistently outperforms the benchmarks across the real-world datasets in predicting correspondences generated by the algorithm.

Method	Synthetic				KITTI @ 1.6 m				KITTI @ 11.3 m				KITTI @ 24 m			
	F1	A	P	R	F1	A	P	R	F1	A	P	R	F1	A	P	R
NAR-P2Pv1	0.30	0.63	0.29	0.31	0.63	0.80	0.63	0.62	0.31	0.63	0.30	0.31	0.29	0.62	0.28	0.30
NAR-P2Pv2	0.18	0.56	0.17	0.19	0.78	0.88	0.79	0.77	0.39	0.69	0.38	0.42	0.42	0.69	0.43	0.40
NAR-P2L	0.09	0.52	0.10	0.09	0.52	0.75	0.53	0.52	0.10	0.52	0.10	0.10	0.11	0.52	0.11	0.10
NAR-GICP	0.16	0.56	0.15	0.17	0.47	0.72	0.48	0.47	0.11	0.53	0.11	0.11	0.20	0.57	0.20	0.20

is significantly larger, and thus, the underlying algorithm might underperform while the NAR-*ICP equivalent is performing better. Our results demonstrate the strong generalisation capabilities and robust performance of our method compared to the algorithms when trained to execute the latter on various challenging data points.

We additionally compare the performance of the algorithmic execution after ground truth optimisation, as shown in Table 3, to demonstrate the performance enhancement of our method. Here, even though we slightly diverge from the original algorithm, we retain its core computational properties while improving its accuracy. Notably, the registration performance across all benchmarks improves significantly in our testing dataset and even becomes comparable across the board, as reflected in Table 3, compared to training without this step in Table 2. This improvement is particularly significant for the pointcloud registration task, as the optimisation step not only approximates the original algorithm but also substantially boosts its performance.

Lastly, our results in Table 4 indicate that the performance of NAR-P2Pv1 and NAR-P2Pv2 is comparable when approximating the output of the algorithms, in RTE^T and RRE^T , while both consistently outperform the other benchmarks. Notably, despite both NAR-P2Pv1 and NAR-P2Pv2 being trained on the same ICP-P2P algorithm, the two-phase approximation in NAR-P2Pv2 leads to slightly inferior performance. This behaviour is expected, as NAR-P2Pv2 approximates a more complex algorithmic trajectory compared to NAR-P2Pv1. By emulating the complete behaviour of the algorithm, NAR-P2Pv2 presents a more intricate and, therefore, interesting benchmark than NAR-P2Pv1. However, despite not approximating the internal algorithmic computations, NAR-P2Pv1 remains a valuable baseline as it is learning to approximate the direct algorithmic outputs at each iteration. This makes NAR-P2Pv1 easier to integrate as a subcomponent within larger learning systems.

Quantitative Results: Intermediate Hints. To assess the performance of our method in approximating the algorithm, we extract the MSE^t error for the intermediate algorithmic steps, as shown in Figure 3. As expected, NAR-P2Pv1 consistently outperforms the other benchmarks as it learns a simpler algorithmic trajectory. Among the more complex benchmarks, NAR-P2Pv2, NAR-P2L, and NAR-GICP, NAR-P2L achieves the lowest medians and IQRs, indicating better model performance in terms of error variance. However, the significant number of outliers in NAR-P2L suggests that the model is far less reliable due to its extreme prediction errors. In contrast, NAR-GICP has almost zero outliers, resulting in consistent and stable performance across predictions, which is preferable for our task. NAR-P2Pv2 demonstrates low medians and IQRs, suggesting good overall performance and reduced error variability, but the presence of outliers in some datasets makes it less reliable than NAR-GICP. Notably, NAR-GICP stands out as the most reliable benchmark for datasets with larger relative displacements, whereas NAR-P2Pv2 excels in scenarios with smaller relative displacements. Across all datasets, the benchmarks performed best on the KITTI @ 1.6 m dataset, highlighting the algorithms' effectiveness on pointclouds with smaller relative displacements.

Quantitative Results: Prediction Accuracy. To further evaluate the performance of our methods in predicting algorithmic outputs, we compare the MSE^T scores and classification metrics, $F1^T$, P^T , R^T , and A^T , across our datasets. Our results in Table 5 demonstrate that NAR-P2Pv1, NAR-P2Pv2, and NAR-P2L achieve comparable performance in predicting the transformed pointclouds. However, as shown in Table 6, NAR-P2Pv2 outperforms the benchmarks in predicting the correspondences on the real-world datasets, while NAR-P2Pv1 excels on the synthetic dataset. Notably, our methods achieve superior performance in the KITTI @ 1.6 m dataset, where the displacement between pointclouds is minimal compared to the others. This observation aligns with the known limitations of ICP-based algorithms, which typically underperform on datasets

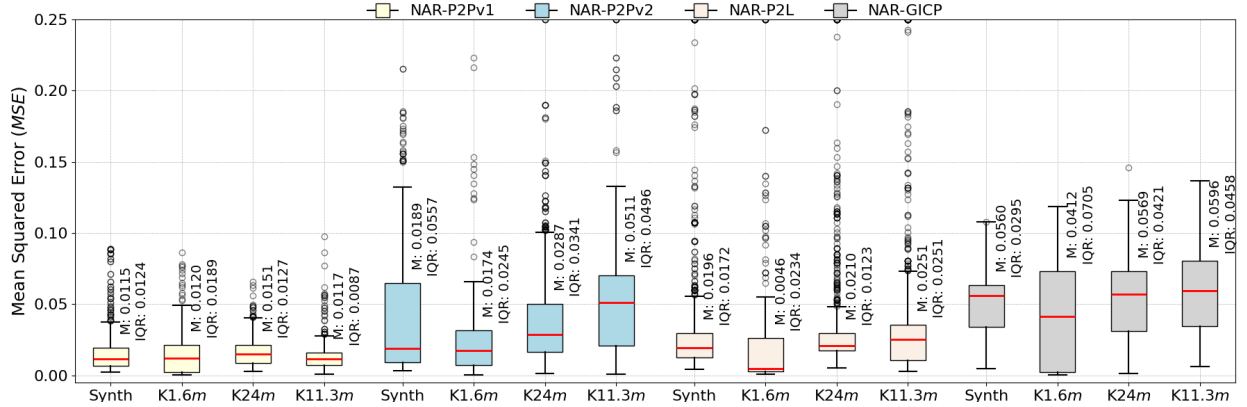


Figure 3. Error distributions, in MSE^t (↓), of the predicted transformed pointclouds during algorithmic execution at each intermediate step across all benchmarks. The box plots visualise the MSE^t distributions (with outliers capped at 0.25 for clarity), the median error, and the interquartile range (IQR).

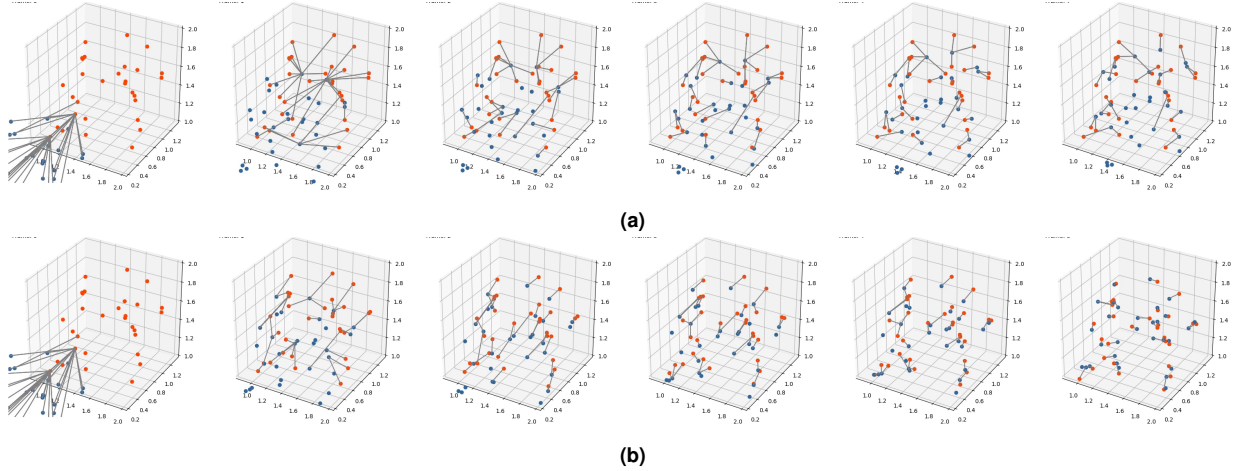


Figure 4. Visualisation of the intermediate steps output for (a) P2P-ICP and (b) ours, NAR-P2Pv2. Despite being trained on the latter, NAR-P2Pv2 demonstrates superior registration performance, achieving better pointcloud alignment and finding stronger correspondences due to the network’s generalisation capabilities. To simplify the visualisation, we use the predictions for the `phase` hint to identify the intermediate algorithmic components and display those from the second phase of the algorithm.

with larger displacement errors. Consequently, the observed performance degradation in such cases may be attributed to the instability of the underlying algorithms.

Qualitative Results. We visualise the registration performance of the algorithmic execution in comparison to the baseline algorithm in Figure 4. Here, we use the same set of pointclouds from the testing set of the synthetic dataset and demonstrate that NAR-P2Pv2 achieves smoother registration performance than the baseline algorithm in the challenging synthetic dataset, highlighting its strong generalisation capabilities. Additionally, while P2P-ICP requires an accurate first initialisation step, making it sensitive to the initial guess, NAR-P2Pv2 learns the initialisation as part of the algorithmic trajectory, leading to more reliable results without the need for this first manual estimation. Notably, the visualisation illustrates that while the baseline P2P-ICP struggles to find strong correspondences and converge, NAR-P2Pv2 – despite being trained on P2P-ICP – successfully identifies strong correspondences and achieves more accurate pointcloud registration than the algorithm. These results highlight the effectiveness and promise of our approach in addressing challenging robotics tasks using neural networks while

maintaining the compositionality and interpretability of the algorithms.

6.2 Optimisation of Neural Execution

A significant advantage of the algorithmic execution over the algorithms is that we can further improve their performance by adding a ground truth optimisation step. To evaluate the effectiveness of adding this step in NAR, we compared the predicted outputs after optimisation with the outputs of the baseline algorithms. Our results in Table 7 and Table 8 demonstrate that the optimised NAR-*ICP models consistently outperform the benchmarks across all datasets, both in predicting the ground truth transformed pointclouds and in identifying the correct correspondences. This is indicated by the significantly lower MSE^{GT} scores and substantially improved classification metrics, $F1^{GT}$, P^{GT} , R^{GT} , and A^{GT} .

6.3 Termination and Runtime Performance

We finally evaluate the effectiveness of our added termination criterion, `stop`, in comparison to the final step from the CLRS Benchmark. In particular, as the number of hints directly dictates the number of processor iterations

Table 7. $MSE^{\text{GT}} (\times 10^2) (\downarrow)$ of the predicted final transformed pointclouds after ground truth optimisation compared to the algorithmic output, against the ground truth. This step significantly improves the performance of the algorithmic execution, surpassing the baseline algorithms across all datasets.

Method	Synthetic			KITTI @ 1.6 m			KITTI @ 11.3 m			KITTI @ 24 m		
	MSE_x	MSE_y	MSE_z	MSE_x	MSE_y	MSE_z	MSE_x	MSE_y	MSE_z	MSE_x	MSE_y	MSE_z
P2P-ICP	6.568	7.874	4.469	3.268	2.524	2.743	9.288	10.516	4.361	8.822	8.697	4.225
NAR-P2Pv1 ⁺	1.101	1.169	0.072	0.764	0.592	0.068	1.203	1.420	0.035	1.163	0.991	0.027
P2P-ICP	6.568	7.874	4.469	3.268	2.524	2.743	9.288	10.516	4.361	8.822	8.697	4.225
NAR-P2Pv2 ⁺	1.117	1.115	0.101	0.625	0.709	0.066	0.902	1.203	0.104	1.075	1.212	0.178
P2L-ICP	4.655	4.924	4.724	2.281	1.888	2.129	4.444	4.598	5.031	4.484	5.461	4.783
NAR-P2L ⁺	1.355	1.354	0.088	0.806	0.533	0.140	1.410	1.391	0.168	1.508	1.422	0.115
G-ICP	10.106	9.911	5.727	6.498	4.889	3.980	9.327	11.122	7.104	9.250	9.712	5.964
NAR-GICP ⁺	1.302	1.157	0.065	0.662	0.655	0.037	1.587	1.412	0.275	0.913	0.848	0.139

Table 8. Classification scores (\uparrow), $F1^{\text{GT}}$, P^{GT} , R^{GT} , and A^{GT} , of the predicted final correspondences after ground truth optimisation compared to the algorithmic output, against the ground truth. The optimisation step significantly improves algorithmic performance in finding strong registration correspondences.

Method	Synthetic				KITTI @ 1.6 m				KITTI @ 11.3 m				KITTI @ 24 m			
	F1	A	P	R	F1	A	P	R	F1	A	P	R	F1	A	P	R
P2P-ICP	0.28	0.63	0.26	0.30	0.51	0.75	0.50	0.53	0.14	0.55	0.13	0.16	0.15	0.56	0.14	0.18
NAR-P2Pv1 ⁺	0.99	0.99	0.98	0.99	0.81	0.91	0.81	0.82	0.96	0.98	0.95	0.97	0.96	0.99	0.95	0.97
P2P-ICP	0.28	0.63	0.26	0.30	0.51	0.75	0.50	0.53	0.14	0.55	0.13	0.16	0.15	0.56	0.14	0.18
NAR-P2Pv2 ⁺	1.00	1.00	1.00	1.00	0.76	0.89	0.74	0.79	0.94	0.97	0.92	0.95	0.96	0.98	0.95	0.97
P2L-ICP	0.04	0.50	0.03	0.06	0.49	0.73	0.48	0.50	0.06	0.51	0.05	0.08	0.05	0.50	0.04	0.07
NAR-P2L ⁺	0.99	1.00	0.99	1.00	0.84	0.92	0.84	0.85	0.89	0.95	0.87	0.91	0.94	0.98	0.92	0.96
G-ICP	0.16	0.56	0.15	0.18	0.39	0.68	0.38	0.40	0.08	0.52	0.07	0.10	0.11	0.53	0.10	0.12
NAR-GICP ⁺	0.99	1.00	0.99	0.99	0.80	0.90	0.78	0.82	0.89	0.96	0.86	0.92	0.87	0.94	0.85	0.90

Table 9. Performance comparison of the output at the predicted termination iteration (stop) and at the last iteration from CLRS (last), measured in average MSE^T . The output from our termination step consistently outperforms the output from the last step.

Method	Synthetic		KITTI @ 1.6 m		KITTI @ 11.3 m		KITTI @ 24 m	
	last	stop	last	stop	last	stop	last	stop
NAR-P2Pv1	0.028	0.021	0.018	0.008	0.033	0.018	0.031	0.023
NAR-P2Pv2	0.043	0.047	0.018	0.007	0.053	0.019	0.039	0.028
NAR-P2L	0.019	0.019	0.009	0.009	0.025	0.027	0.021	0.024
NAR-GICP	0.054	0.050	0.029	0.028	0.056	0.051	0.051	0.047

in CLRS, we evaluate the effectiveness of introducing the termination network with respect to prediction accuracy, runtime performance, and the number of steps. We first assess the average MSE of the transformed pointclouds at the termination step (stop) and the output of the algorithm, alongside the average MSE from the last step from CLRS (last) and the output of the algorithm, as seen in Table 9. Our results demonstrate that the results from the predicted termination step are consistently superior to, or at least comparable, across all datasets and benchmarks.

We additionally compare the total runtime and the average number of steps for each algorithm and its corresponding algorithmic execution, with (stop) and without (last) termination, as shown in Table 10. To ensure a fair comparison between benchmarks, the average number of steps is calculated solely on those from the second phase of the algorithm, as predicted from the `phase` hint. Notably, the NAR-*ICP models reduce the runtime of P2L-ICP

and G-ICP, which require additional computations, such as the estimation of normals and covariances, naturally resulting in longer execution times. Our models address and mitigate this drawback, leading to improved efficiency. Additionally, in almost all cases, our method requires fewer execution steps to achieve the desired algorithmic output compared to the baseline algorithms. Across all datasets, by adding the termination, we not only reduce runtime but we significantly enhance the models' accuracy in approximating the algorithmic steps. These position NAR-*ICP as a good alternative compared to traditional *ICP methods, especially in time-sensitive applications.

7 Ablation

To find the optimal processor architecture, hints configuration, and teacher forcing probability, we compared the performance of each configuration on the metrics defined in

Table 10. Runtime performance and average number of steps comparison for each algorithm and their respective algorithmic execution through NAR at the last step of CLRS (last) and the predicted termination step (stop). Our termination significantly improves the total runtime and the average number of steps requirements for our models.

	Total Time [s]	Avg. Steps
P2P-ICP	0.051	10
NAR-P2Pv1 ⁺ (last)	0.142	15
NAR-P2Pv1 ⁺ (stop)	0.064	7
P2P-ICP	0.051	10
NAR-P2Pv2 ⁺ (last)	0.172	37
NAR-P2Pv2 ⁺ (stop)	0.069	15
P2L-ICP	0.078	28
NAR-P2L ⁺ (last)	0.270	98
NAR-P2L ⁺ (stop)	0.046	17
G-ICP	0.946	32
NAR-GICP ⁺ (last)	0.268	98
NAR-GICP ⁺ (stop)	0.056	21

Section 5.3, using the synthetic dataset and P2P-ICP as the baseline.

Processors. We tested the following processors on the synthetic dataset using the CLRS Benchmark (Veličković et al. 2022): (a) Pointer-Graph Network (PGN) (Veličković et al. 2020), (b) Graph Attention Network (GAT) (Veličković et al. 2018), (c) Triplet-Message-Passing Neural Network (MPNN) (Ibarz et al. 2022), (d) GATv2 (Brody et al. 2022), and (e) MPNN (Gilmer et al. 2017). Our results in Table 11 demonstrate that the MPNN-based models performed best, with the Triplet-MPNN mostly outperforming the MPNN. As expected, the Triplet-MPNN performed better at also predicting the correspondences in both cases. By comparing the median and IQR in Figure 5, we concluded that the Triplet-MPNN achieved the best performance trade-off in predicting the intermediate steps, as indicated by its low median and IQR along with the very small number of outliers.

Teacher Forcing Probability. Given the nature of the teacher-forcing optimisation, we are primarily interested in the model’s performance at predicting the transformed pointclouds at each intermediate step. To select the optimal probability threshold, P_T , we compared different threshold values against the model’s output. Comparing the model’s predictive performance for each, as seen in Figure 6, we concluded that the optimal probability threshold is $P_T = 0.1$

Table 11. Ablation study of different model architectures, comparing average MSE (\downarrow) scores for the predicted transformed pointclouds, along with F1 (\uparrow) and balanced accuracy A (\uparrow) for the predicted correspondences.

	NAR-P2Pv2 ⁺			NAR-P2Pv2		
	MSE ^{GT}	F1 ^{GT}	A ^{GT}	MSE ^T	F1 ^T	A ^T
PGN	0.010	0.62	0.84	0.050	0.04	0.49
GAT-Full	0.008	0.56	0.81	0.045	0.22	0.59
Triplet-MPNN	0.007	0.99	0.99	0.017	0.30	0.63
GATv2-Full	0.009	0.54	0.80	0.035	0.24	0.60
MPNN	0.002	0.82	0.93	0.038	0.26	0.60

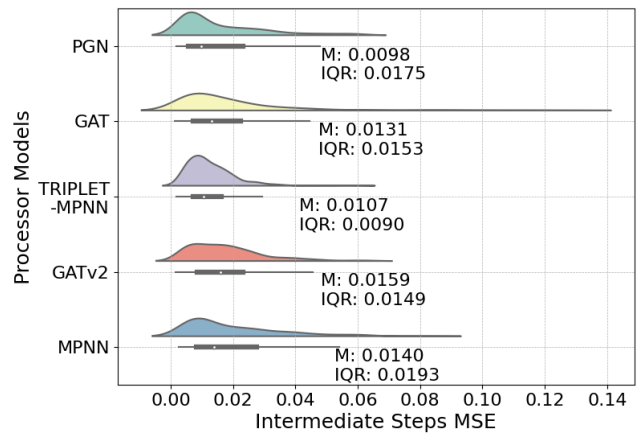


Figure 5. Ablation study of different model architectures, comparing the $MSE^t(\downarrow)$ error distributions of intermediate steps predictions.

as it achieves the lowest median and the smallest IQR while maintaining a relatively small number of outliers.

Hint Configuration. We tested various hint configurations to determine the optimal setup for capturing the trajectory of the algorithm. Each configuration varies in the selection of intermediate algorithmic steps that are passed as hints to the processor. We evaluated our model’s performance against the following hint configurations:

1. P2: Pass only the output of the second phase of the algorithm.
2. P12: Pass the output of both phases of the algorithm.
3. P1I: Pass the intermediate calculations of the first phase of the algorithm - i.e. the correspondence-finding iterations.
4. P1I2: Pass the intermediate calculations of the first phase of the algorithm along with the output of the second phase.

Here, we initially quantitatively evaluate the final predictions from the models, as shown in Table 12. The results demonstrate that different hint configurations achieve comparable performance in predicting the final output of

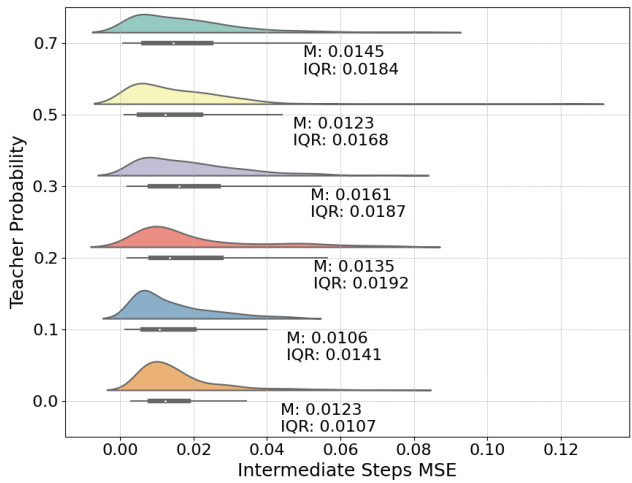


Figure 6. Ablation study of different teacher probability values, comparing the $MSE^t(\downarrow)$ error distributions of intermediate steps predictions.

Table 12. Ablation study of different hint configurations for baseline NAR-P2P. **Bold** and underline values indicate the best and second-best results, respectively. We compare average $MSE(\downarrow)$ for the predicted transformed pointclouds, along with $F1(\uparrow)$ and balanced accuracy $A(\uparrow)$ for the predicted correspondences.

	NAR-P2P ⁺			NAR-P2P		
	MSE^{GT}	$F1^{GT}$	A^{GT}	MSE^T	$F1^T$	A^T
P2	<u>0.011</u>	0.93	0.97	0.029	0.26	<u>0.61</u>
P12	0.008	<u>0.95</u>	<u>0.98</u>	<u>0.049</u>	0.21	0.58
P1I	0.016	1.00	1.00	0.09	<u>0.35</u>	<u>0.61</u>
P1I2	0.014	1.00	1.00	0.058	0.43	0.66

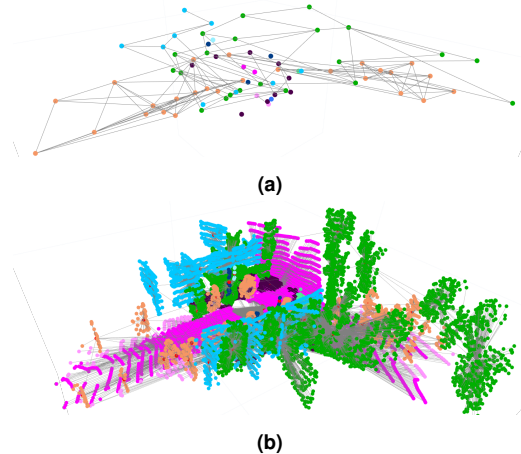


Figure 7. Example of one scan from the real-world dataset, with the centroids in (a) and the corresponding pointclouds in (b), where each object's sub-pointcloud is coloured differently.

the algorithm and the ground truth, with P2 and P12 outperforming the others in predicting the transformed pointclouds, as indicated by lower average MSE scores. Our experiments indicate that to effectively learn the intermediate representations of the algorithms, hints should be representative of the algorithm's entire trajectory. However, when the changes between the hints are minimal and the inputs are imbalanced – such as in the cases of P1I and P1I2 – the model's performance suffers in predicting the intermediate hints. For configurations P1I and P1I2, the intermediate ground truth hints are mostly repetitive, and the changes between scalar hints are minimal. Therefore, we concluded that the configurations P2 and P12 are of most interest and as such, they have both been explored further above in NAR-P2Pv1 and NAR-P2Pv2, respectively.

8 Integration of NAR-*ICP in Learning Pipelines

This section describes how NAR-*ICP can be used as a sub-component of a larger learning pipeline. To demonstrate its successful integration, we developed a contrastive learning framework that generates latent feature representations of objects in SemanticKITTI (Behley et al. 2019). These learned representations then serve as input to the processor in NAR-*ICP, indicating its effectiveness in leveraging latent features rather than relying solely on Cartesian data, which is typical for traditional ICP-based algorithms.

To achieve this, we learn a useful embedding representation for each object in the real-world dataset to facilitate registration. In particular, we leverage a contrastive learning framework Chen et al. (2020a) along with a GNN to generate strong embedding representations for each object, which are then used as input $x_i^{(t)}$ to our approach. This contrastive approach is particularly effective in distinguishing between similar and dissimilar data points, facilitating robust feature learning for registration. Figure 7 illustrates the approach, depicting both the centroids used for registration and the points associated with each object, which are then used to extract their latent feature representations. Our results in Table 13 and Table 14 demonstrate that our combined contrastive and NAR framework achieves performance comparable to NAR-*ICP trained on Cartesian data, highlighting the ease of integrating NAR-*ICP into training pipelines.

Registration algorithms work well with three-dimensional pointclouds, while high-level semantics and learned embeddings are incorporated into learned methods but not directly into the calculations. This integration experiment is interesting as it presents noisy and complex data in the input of the algorithmic execution and demonstrates that we can incorporate semantics and latent features when solving ICP-based algorithms. This framework is used to demonstrate the flexibility and generalisability of our method as well as its usefulness as a fully differential component of a larger learning system.

9 Conclusion and Future Directions

This work proposes a novel NAR-based approach for learning to approximate the intermediate steps of ICP-based algorithms, extending the CLRS Benchmark into the field of robotics. Our method not only mimics pointcloud registration pipelines but also consistently outperforms them. We additionally demonstrate the robustness and flexibility of NAR-*ICP when handling noisy and complex data.

Table 13. Registration performance of the integrated learning pipeline for the final step of NAR-*ICP models compared to the final step of the algorithm and the ground truth in $RTE^T(\downarrow)$, $RRE^T(\downarrow)$ and $RTE^{GT}(\downarrow)$, $RRE^{GT}(\downarrow)$, $RTE^{GT}(\downarrow)$, respectively.

Method	RTE^T	RRE^T	RTE^{GT}	RRE^{GT}
NAR-P2Pv1	0.818	1.384	1.014	1.998
NAR-P2Pv2	0.821	1.442	1.167	2.127
NAR-P2L	1.208	2.201	0.783	1.338
NAR-GICP	0.881	1.644	0.935	2.016

Table 14. Prediction performance of the integrated learning pipeline for the NAR-*ICP models after ground truth optimisation, evaluated using $RTE^{GT}(\downarrow)$ and $RRE^{GT}(\downarrow)$ for registration performance, average $MSE^{GT}(\downarrow)$ for the predicted transformed pointclouds, and $F1^{GT}(\uparrow)$ and balanced accuracy $A^{GT}(\uparrow)$ for correspondences.

Method	RTE	RRE	MSE	$F1$	A
NAR-P2Pv1 ⁺	0.555	1.004	0.012	0.64	0.82
NAR-P2Pv2 ⁺	0.596	1.058	0.023	0.64	0.82
NAR-P2L ⁺	0.621	1.151	0.026	0.54	0.78
NAR-GICP ⁺	0.507	0.937	0.019	0.63	0.82

The NAR framework is further extended by leveraging the specific architecture of the ICP-based algorithms, enhancing its functionality and showcasing its effectiveness in approximating complex multi-step algorithms.

Our method aims to advance current robotics systems by proposing a more interpretable and efficient learning framework. By integrating classical algorithms with deep learning, we combine structured reasoning and logical computations with the adaptability and generalisation capabilities of neural networks. NAR-based models provide access to their intermediate computations, leading to more reliable, robust, and transparent robotics systems. As such, we foresee that learning in the space of autonomous navigation, planning, and manipulation will reveal interesting applications of NAR, extending NAR-^{*}ICP and the CLRS Benchmark further. Furthermore, the inherent interpretability of NAR can enhance human-robot interaction by enabling systems to explain their decision-making process, leading to more transparent and reliable systems for real-world applications.

Acknowledgements

We particularly thank Jake Bruce and Simon Osindero for their valuable comments on this work and for reviewing the paper prior to submission. We also thank Benjamin Ramtoula for the discussions leading up to the submission.

Funding

Efimia Panagiotaki was supported by a DeepMind Engineering Science Research Scholarship, University of Oxford. This work was partially supported by the EPSRC RAILS project (grant reference: EP/W011344/1).

References

Amberg B, Romdhani S and Vetter T (2007) Optimal step nonrigid icp algorithms for surface registration. In: *2007 IEEE Conference on Computer Vision and Pattern Recognition*. pp. 1–8. DOI:10.1109/CVPR.2007.383165.

Bai H (2023) ICP Algorithm: Theory, Practice and Its SLAM-oriented Taxonomy. *Applied and Computational Engineering* 2(1): 10–21. DOI:10.54254/2755-2721/2/ojs/20220512.

Behley J, Garbade M, Milioto A, Quenzel J, Behnke S, Stachniss C and Gall J (2019) SemanticKITTI: A dataset for semantic scene understanding of LiDAR sequences. *Proceedings of the IEEE International Conference on Computer Vision 2019-October(iii)*: 9296–9306. DOI:10.1109/ICCV.2019.00939.

Billard A and Grollman D (2012) *Imitation Learning in Robots*. Boston, MA: Springer US. ISBN 978-1-4419-1428-6, pp. 1494–1496. DOI:10.1007/978-1-4419-1428-6_758. URL https://doi.org/10.1007/978-1-4419-1428-6_758.

Bounsi W, Ibarz B, Dudzik A, Hamrick JB, Markeeva L, Vitvitskyi A, Pascanu R and Veličković P (2024) Transformers meet neural algorithmic reasoners. URL <https://arxiv.org/abs/2406.09308>.

Brody S, Alon U and Yahav E (2022) How attentive are graph attention networks? In: *International Conference on Learning Representations*. URL <https://openreview.net/forum?id=F72ximsx7C1>.

Celemin C, Pérez-Dattari R, Chisari E, Franzese G, de Souza Rosa L, Prakash R, Ajanović Z, Ferraz M, Valada A and Kober J (2022) Interactive imitation learning in robotics: A survey. URL <https://arxiv.org/abs/2211.00600>.

Chen T, Kornblith S, Norouzi M and Hinton G (2020a) A simple framework for contrastive learning of visual representations. *arXiv preprint arXiv:2002.05709*.

Chen Y, Wu L and Zaki MJ (2020b) Iterative deep graph learning for graph neural networks: Better and robust node embeddings. *Advances in Neural Information Processing Systems* 2020-Decem(NeurIPS).

Deac A, Veličković P, Milinković O, Bacon PL, Tang J and Nikolić M (2020) XLVIN: eXecuted Latent Value Iteration Nets : 1–18URL <https://arxiv.org/abs/2010.13146>.

Deac A, Veličković P, Milinković O, Bacon PL, Tang J and Nikolić M (2021) Neural Algorithmic Reasoners are Implicit Planners. *Advances in Neural Information Processing Systems* 19(c): 15529–15542.

Dudzik A and Veličković P (2022) Graph neural networks are dynamic programmers. URL <https://arxiv.org/abs/2203.15544>.

Firoozi R, Tucker J, Tian S, Majumdar A, Sun J, Liu W, Zhu Y, Song S, Kapoor A, Hausman K, Ichter B, Driess D, Wu J, Lu C and Schwager M (2023) Foundation models in robotics: Applications, challenges, and the future. URL <https://arxiv.org/abs/2312.07843>.

Geiger A, Lenz P, Stiller C and Urtasun R (2013) Vision meets robotics: The kitti dataset. *The International Journal of Robotics Research* 32(11): 1231–1237. DOI:10.1177/0278364913491297. URL <https://doi.org/10.1177/0278364913491297>.

Georgiev D, Barbiero P, Kazhdan D, Veličković P and Liò P (2022) Algorithmic Concept-Based Explainable Reasoning. *Proceedings of the 36th AAAI Conference on Artificial Intelligence, AAAI 2022* 36: 6685–6693. DOI:10.1609/aaai.v36i6.20623.

Gilmer J, Schoenholz SS, Riley PF, Vinyals O and Dahl GE (2017) Neural message passing for quantum chemistry. URL <https://arxiv.org/abs/1704.01212>.

Glorot X and Bengio Y (2010) Understanding the difficulty of training deep feedforward neural networks. In: Teh YW and Titterington M (eds.) *Proceedings of the Thirteenth International Conference on Artificial Intelligence and Statistics, Proceedings of Machine Learning Research*, volume 9. Chia Laguna Resort, Sardinia, Italy: PMLR, pp. 249–256. URL <https://proceedings.mlr.press/v9/glorot10a.html>.

Godwin J, Schaarschmidt M, Gaunt AL, Sanchez-Gonzalez A, Rubanova Y, Veličković P, Kirkpatrick J and Battaglia P (2022) Simple GNN regularisation for 3d molecular property prediction and beyond. In: *International Conference on Learning Representations*. URL <https://openreview.net/forum?id=1wVvweK3oIb>.

Hamrick JB, Allen KR, Bapst V, Zhu T, McKee KR, Tenenbaum JB and Battaglia PW (2018) Relational inductive bias for physical construction in humans and machines. URL <https://arxiv.org/abs/1806.01203>.

He Y, Veličković P, Liò P and Deac A (2022) Continuous Neural Algorithmic Planners. *Proceedings of Machine Learning Research* 198(LoG).

Ibarz B, Kurin V, Papamakarios G, Nikiforou K, Bennani M, Csordás R, Dudzik A, Bošnjak M, Vitvitskyi A, Rubanova Y, Deac A, Bevilacqua B, Ganin Y, Blundell C and Veličković P (2022) A Generalist Neural Algorithmic Learner. *Proceedings of Machine Learning Research* 198(Log).

Kober J, Bagnell JA and Peters J (2013) Reinforcement learning in robotics: A survey. *The International Journal of Robotics Research* 32(11): 1238–1274. DOI:10.1177/0278364913495721. URL <https://doi.org/10.1177/0278364913495721>.

Kong X, Yang X, Zhai G, Zhao X, Zeng X, Wang M, Liu Y, Li W and Wen F (2020) Semantic graph based place recognition for 3D point clouds. *IEEE International Conference on Intelligent Robots and Systems* (September): 8216–8223. DOI:10.1109/IROS45743.2020.9341060.

Li H, Sumner RW and Pauly M (2008) Global correspondence optimization for non-rigid registration of depth scans. *Computer Graphics Forum* 27. URL <https://api.semanticscholar.org/CorpusID:17982667>.

Lu W, Wan G, Zhou Y, Fu X, Yuan P and Song S (2019) Deepvcp: An end-to-end deep neural network for point cloud registration. In: *2019 IEEE/CVF International Conference on Computer Vision (ICCV)*. IEEE. DOI:10.1109/iccv.2019.00010. URL <http://dx.doi.org/10.1109/ICCV.2019.00010>.

McKay N PB (1992) A Method for Registration of 3D Shapes. *IEEE Trans. on Pattern Analysis and Machine Intelligence (TPAMI)* 14(2):239.

Mendes E, Koch P and Lacroix S (2016) Icp-based pose-graph slam. In: *2016 IEEE International Symposium on Safety, Security, and Rescue Robotics (SSRR)*. pp. 195–200. DOI:10.1109/SSRR.2016.7784298.

Numeroso D, Bacciu D and Veličković P (2023) Dual Algorithmic Reasoning : 1–16URL <http://arxiv.org/abs/2302.04496>.

Panagiotaki E, De Martini D, Pramatarov G, Gadd M and Kunze L (2023) Sem-gat: Explainable semantic pose estimation using learned graph attention. In: *2023 21st International Conference on Advanced Robotics (ICAR)*. pp. 367–374. DOI:10.1109/ICAR58858.2023.10407013.

Pascanu R, Mikolov T and Bengio Y (2013) On the difficulty of training recurrent neural networks. In: Dasgupta S and McAllester D (eds.) *Proceedings of the 30th International Conference on Machine Learning, Proceedings of Machine Learning Research*, volume 28. Atlanta, Georgia, USA: PMLR, pp. 1310–1318. URL <https://proceedings.mlr.press/v28/pascanu13.html>.

Pistilli F and Averta G (2023) Graph learning in robotics: a survey. URL <https://arxiv.org/abs/2310.04294>.

Pomerleau F, Colas F, Siegwart R and Magnenat S (2013) Comparing ICP variants on real-world data sets: Open-source library and experimental protocol. *Autonomous Robots* 34(3): 133–148. DOI:10.1007/s10514-013-9327-2.

Pramatarov G, Gadd M, Newman P and Martini DD (2024) That's my point: Compact object-centric lidar pose estimation for large-scale outdoor localisation. URL <https://arxiv.org/abs/2403.04755>.

Qin Z, Yu H, Wang C, Guo Y, Peng Y and Xu K (2022) Geometric transformer for fast and robust point cloud registration. URL <https://arxiv.org/abs/2202.06688>.

Rusinkiewicz S and Levoy M (2001) Efficient variants of the ICP algorithm. *Proceedings of International Conference on 3-D Digital Imaging and Modeling, 3DIM* : 145–152DOI:10.1109/IM.2001.924423.

Saleh AR and Momeni HR (2024) An improved iterative closest point algorithm based on the particle filter and K-means clustering for fine model matching. *Visual Computer* DOI: 10.1007/s00371-023-03195-0. URL <https://doi.org/10.1007/s00371-023-03195-0>.

Segal AV, Haehnel D and Thrun S (2010) Generalized-ICP. *Robotics: Science and Systems* 5: 161–168. DOI:10.15607/rss.2009.v.021.

Shi C, Chen X, Huang K, Xiao J, Lu H and Stachniss C (2021) Keypoint matching for point cloud registration using multiplex dynamic graph attention networks. *IEEE Robotics and Automation Letters* 6(4): 8221–8228. DOI:10.1109/LRA.2021.3097275.

Singh B, Kumar R and Singh VP (2022) Reinforcement learning in robotic applications: a comprehensive survey. *Artificial Intelligence Review* 55: 945–990. DOI:10.1007/s10462-021-09997-9. URL <https://doi.org/10.1007/s10462-021-09997-9>.

Veličković P, Badia AP, Budden D, Pascanu R, Banino A, Dashevskiy M, Hadsell R and Blundell C (2022) The CLRS Algorithmic Reasoning Benchmark. *Proceedings of Machine Learning Research* 162: 22084–22102.

Veličković P and Blundell C (2021) Neural algorithmic reasoning. *Patterns* 2(7): 1–7. DOI:10.1016/j.patter.2021.100273.

Veličković P, Ying R, Padovano M, Hadsell R and Blundell C (2020) Neural Execution of Graph Algorithms. *8th International Conference on Learning Representations, ICLR 2020* .

Veličković P, Buesing L, Overlan MC, Pascanu R, Vinyals O and Blundell C (2020) Pointer graph networks. URL <https://arxiv.org/abs/2006.06380>.

Veličković P, Cucurull G, Casanova A, Romero A, Liò P and Bengio Y (2018) Graph attention networks. URL <https://arxiv.org/abs/1710.10903>.

Vizzo I, Guadagnino T, Mersch B, Wiesmann L, Behley J and Stachniss C (2023) Kiss-icp: In defense of point-to-point icp – simple, accurate, and robust registration if done the right way. *IEEE Robotics and Automation Letters* 8(2): 1029–1036. DOI:10.1109/lra.2023.3236571. URL <http://dx.doi.org/10.1109/LRA.2023.3236571>.

Wang Y and Solomon JM (2019) Deep closest point: Learning representations for point cloud registration. URL <https://arxiv.org/abs/1905.03304>.

Xu K, Li J, Zhang M, Du SS, ichi Kawarabayashi K and Jegelka S (2020) What can neural networks reason about? In: *International Conference on Learning Representations*. URL <https://openreview.net/forum?id=rJxbJeHFPS>.

Y Chen and G Medioni (1991) Object modeling by registration of multiple range images. *Proc. of the IEEE/RSJ Int. Conf. on Intelligent Robots and Systems (IROS)* .

Zhang J, Yao Y and Deng B (2021) Fast and robust iterative closest point. *IEEE Transactions on Pattern Analysis and Machine Intelligence* : 1–1DOI:10.1109/tpami.2021.3054619. URL <http://dx.doi.org/10.1109/TPAMI.2021.3054619>.

Zhang Y and Yang Q (2021) A survey on multi-task learning. URL
<https://arxiv.org/abs/1707.08114>.

Zhuang F, Qi Z, Duan K, Xi D, Zhu Y, Zhu H, Xiong H and He Q (2020) A comprehensive survey on transfer learning. URL
<https://arxiv.org/abs/1911.02685>.